Acoust. Sci. & Tech. **39**, 3 (2018)

PAPER

Localization of marine seismic vibrator based on hyperbolic Radon transform

Tsubasa Kusano*, Kohei Yatabe† and Yasuhiro Oikawa‡

Department of Intermedia Art and Science, Waseda University, 3–4–1 Ohkubo, Shinjuku-ku, Tokyo, 169–8555 Japan

(*Received 27 February 2017, Accepted for publication 23 October 2017*)

Abstract: In marine seismic surveys to explore seafloor resources, the structure below the seafloor is estimated from the obtained sound waves, which are emitted by a marine seismic sound source and reflected or refracted between the layers below the seafloor. In order to estimate the structure below the seafloor from returned waves, information of the sound source position and the sound speed are needed. Marine seismic vibrators, which are one of the marine seismic sound sources, have some advantages such as high controllability of the frequency and phase of the sound, and oscillation at a high depth. However, when the sound source position is far from the sea surface, it becomes difficult to specify the exact position. In this paper, we propose a method to estimate the position of a marine seismic vibrator and the sound speed from obtained seismic data by formulating an optimization problem via hyperbolic Radon transform. Numerical simulations confirmed that the proposed method almost achieves theoretical lower bounds for the variances of the estimations.

Keywords: Marine seismic survey, Sound source localization, Gradient-based optimization, Seismic migration, Functional approximation

PACS number: 43.30.Ma, 43.60.Jn [doi:10.1250/ast.39.215]

1. INTRODUCTION

To explore seafloor resources such as petroleum and gas, seismic surveys using sound waves are performed [1–8]. In marine seismic surveys, sound waves are emitted from a seismic sound source and receivers obtain the returned waves, which are reflected or refracted between the layers below the seafloor. Then, the structure below the seafloor is estimated from the obtained data based on the positional relations between the sound source and the receivers, and the sound speed. Therefore, the sound source position and the sound speed are important information for accurate estimation of the structure below the seafloor.

For the marine seismic sound sources, airguns [9,10], which emit sharp pressure pulses by releasing compressed air, are widely used. However, a concern is that the pulsive sounds emitted by airguns can harm marine animals [11,12]. Recently, marine seismic vibrators (MSVs) [13–16], which can control the frequency and phase of the sound with high reproducibility, have been studied as another marine seismic sound source. By producing low-instantaneous-pressure-level, long-duration oscillating signals using an MSV, damage to the marine environment can be reduced in seismic surveys.

Airguns are generally deployed 3–10 m below the water surface [10]. On the other hand, an MSV can be operated at 10–250 m below the water surface by adjusting the internal pressure to the seawater pressure [16]. Thus, since an MSV can oscillate at a position closer to the seafloor, it can reduce the transmission loss of sound waves between the sound source and the seafloor. However, as the MSV position is deeper and further from the sea surface, it is more difficult to specify the exact position. As a current underwater positioning method, an ultra short baseline (USBL) system [17,18], which is one of the acoustic positioning systems, is commonly used with an MSV. Nevertheless, when the sound source position is far from the transceiver array, the measurement accuracy of the position decreases owing to the limitation on the size of the transceiver array [19]. In addition, a USBL system, or any other positioning system, requires the installation of other apparatus, which increases the cost and failure risk even though the source position is not of primary interest. Therefore, it is desirable that the sound source position can be estimated from only the obtained signals without adding any apparatus.

*e-mail: tsubasa.k@suou.waseda.jp
†e-mail: k.yatabe@asagi.waseda.jp
‡e-mail: yoikawa@waseda.jp

To estimate the source position only from observed signals, the time of arrival (TOA) and the time difference of arrival (TDOA) localization methods have been studied [20]. However, accurately detecting the travel time is quite difficult for the situations in which an MSV is employed because (1) the peak of the waveform is dull owing to narrowband signal, whose frequency range is limited by a mechanical issue of the MSV; and (2) the signal-to-noise ratio (SNR) of the observed signal is low, typically under 0 dB, while the travel time is susceptible to noise. Therefore, an estimation method must be robust to noise. As other source localization methods, the beamforming technique has been studied [21]. In particular, matched field processing (MFP) methods, which generalize the beamformer methods by taking the underwater environment into consideration, are widely used in underwater acoustics [22,23]. That is, not only the direction and distance to the sound source but also the sound speed distribution are simultaneously considered in MFP. However, MFP methods usually utilized a predetermined sound speed distribution obtained by measurement or estimation, which can be a critical source of error in position estimation. Moreover, they require an enormous number of calculations to obtain a position because the optimization problem necessary for position estimation is generally solved by an exhaustive search, i.e., every candidate source position is calculated even when the number of sound sources can be assumed to be one.

In this paper, a method for estimating the position of an MSV and the sound speed from obtained marine seismic data is proposed [24]. The important differences between the proposed method and the other methods above are threefold: (1) the sound speed is simultaneously estimated with the position; (2) it is formulated in the time domain to increase the SNR; and (3) an efficient gridless search is attained by gradient-based optimization. The proposed method is formulated as a maximization problem of the hyperbolic Radon transform, where not only the position but also the sound speed is considered as the optimization variable so that the error in the sound speed model is eliminated. By formulating the problem in the time domain, the proposed method takes advantage of the structure of the observed signal, which is pulsive. To optimize the parameter in the time domain, a functional approximation of the data is utilized so that a subsample delay is allowed. Moreover, the gradient of the hyperbolic Radon transform is directly calculated for efficient optimization. An acceleration technique is also employed to improve the accuracy.

2. SEISMIC MIGRATION

Seismic migration is the seismic imaging technique that reveals the subsurface reflector positions [25]. In marine seismic surveys, sound waves are emitted periodically from a source towed by a vessel, and receivers obtain waves reflected from subsurface reflectors below the seafloor. Seismic migration relocates the obtained energy of reflected waves energy to the subsurface reflector positions in the time or space domain based on the preliminarily estimated velocity distribution and the positional relationship between the source and the receivers.

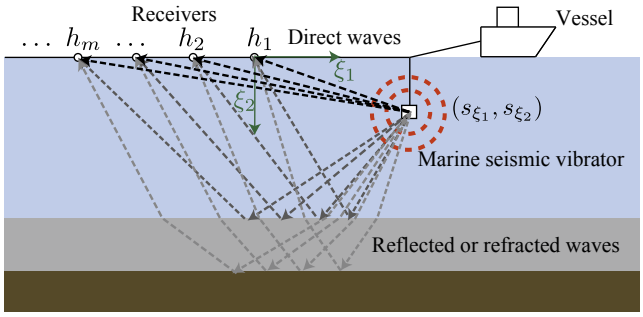

Fig. 1 Positional relationship of MSV and receivers. The vertical positions of the receivers are set to zero.

In this paper, the sound source localization problem in two-dimensional marine seismic surveys using an MSV is considered. Let us assume that the MSV and receivers are distributed as shown in Fig. 1. It is common to consider such horizontally arranged receivers in a two-dimensional marine seismic survey, which aims to image a slice of the subsurface structure [26]. Furthermore, in a marine seismic survey in shallow water (0–300 m), which is the range covered by an MSV, the sound speed can be assumed as a constant since the change in the sound speed with respect to the depth is sufficiently small in this range [27]. Thus, considering the operable depth of an MSV (10–250 m), the sound speed is set to a constant c. Then, sound waves emitted from the MSV are assumed to be spherical waves, and the travel time of a direct wave from the MSV to the mth receiver is formulated as

$$\tau(h_m, \boldsymbol{\theta}) = p\sqrt{(s_{\xi_1} - h_m)^2 + s_{\xi_2}^2}, \tag{1}$$

where $\boldsymbol{s} = [s_{\xi_1}\ s_{\xi_2}]^{\mathrm{T}}$ is the position of the MSV, h_m is the horizontal position of the mth receiver, the vertical positions of the receivers are assumed to be zero, p is the slowness, denoted as the reciprocal of the sound speed c, $\boldsymbol{\theta} = [\boldsymbol{s}^{\mathrm{T}}\ p]^{\mathrm{T}}$ is a parameter to be estimated, and A^{T} denotes the transpose of A.

3. PROPOSED METHOD

We propose a method to estimate the parameter $\boldsymbol{\theta}$ by maximizing the value of the hyperbolic Radon transform. A diagram of the proposed method is illustrated in Fig. 2, where the p-axis is omitted for simplification. First, the parameter estimation problem is formulated as a maximization problem of the hyperbolic Radon transform.

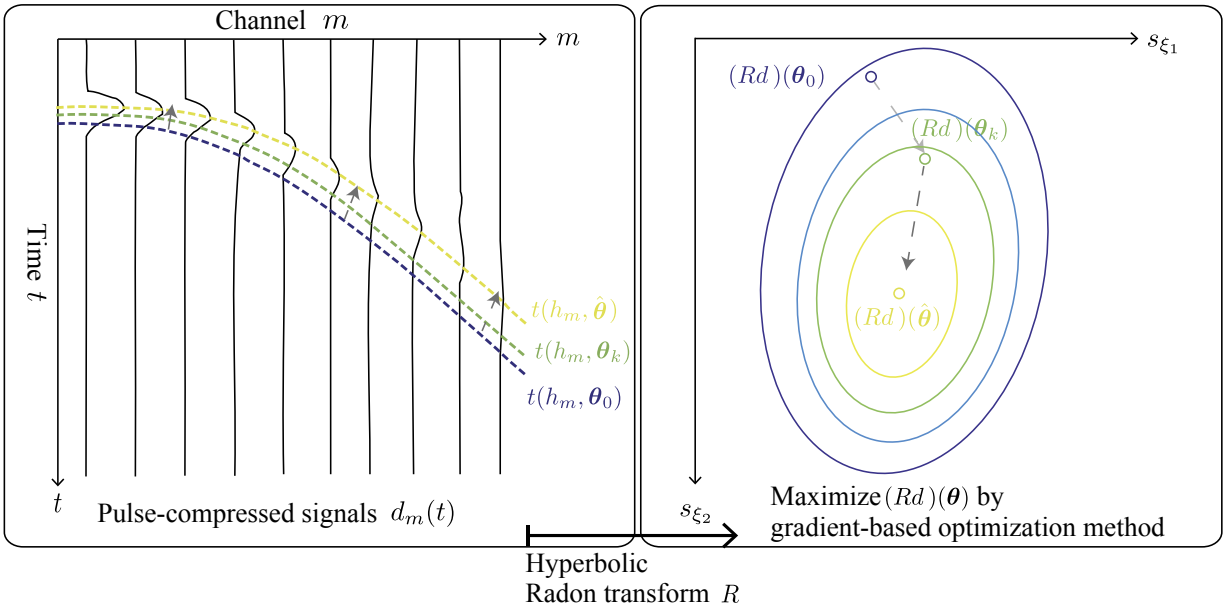

Fig. 2 Diagram of the proposed method.

Then, the maximization problem is solved by a gradient-based optimization method with interpolation using the spherical Bessel function of the first kind.

The assumptions behind the proposed method are (1) observed signals are pulsive; (2) observations are synchronized; and (3) arrival times of direct and reflected sounds are different in the majority of received signals. The first assumption is fulfilled for both an airgun and an MSV because an airgun naturally emits explosive sounds and the signal from an MSV is processed by pulse compression to recover the pulse [28,29]. The second assumption is the usual situation for seismic surveys, especially for those using an MSV. The third assumption is that the direct sound must be distinguishable from the reflected ones, which is usually the case, particularly for the received signals near the sound source.

The proposed method can take advantage of these assumptions by formulating the problem in the time domain. Since a pulse is a signal whose energy is concentrated within a certain time interval, its SNR is high in this interval and low elsewhere. Taking this characteristic of pulse signals into account is not easy for methods in the frequency domain because the energy of a pulse spreads widely along the frequency axis. On the other hand, a formulation based on the hyperbolic Radon transform can easily utilize this energy concentration principle as it is in the time domain. However, a time-domain formulation has to deal with subsample delays (delays less than the sampling interval), which can be handled easily in the frequency domain. The proposed method solves this difficulty by approximating discrete data as a continuous function.

3.1. Parameter Estimation via Hyperbolic Radon Transform

The Radon transform is a transformation via a curvilinear integral along curves characterized by parameters, which was first studied by Johann Radon in 1917 [30]. Since the Radon transform processes multichannel data simply, it is frequently applied to seismic data analysis [31–37].

Let $d(t, \xi_1)$ be pulse-compressed signals obtained from a receiver at horizontal position ξ_1. Here, the Radon transform, which integrates the data $d(t, \xi_1)$ along the hyperbola $\tau(\xi_1, \boldsymbol{\theta})$, is considered. The hyperbolic Radon transform $\mathcal{R}$, which maps the data $d(t, \xi_1)$ to $(\mathcal{R}d)(\boldsymbol{\theta})$, is formulated by

$$(\mathcal{R}d)(\boldsymbol{\theta}) = \int_{h_M}^{h_1} d(\tau(\xi_1, \boldsymbol{\theta}), \xi_1)\, d\xi_1. \tag{2}$$

When the data are obtained from M receivers, the integration of Eq. (2) is approximated by the summation of the data from each receiver,

$$(\mathcal{R}d)(\boldsymbol{\theta}) \simeq (Rd)(\boldsymbol{\theta}) = \sum_{m=1}^{M} d_m(\tau(h_m, \boldsymbol{\theta})), \tag{3}$$

where $d_m(t) = d(t, h_m)$ is the pulse-compressed signal obtained from the mth receiver. Note that although this formula is similar to that of the delay-and-sum beamformer, they are not equivalent because the hyperbolic Radon transform sums only the signals at certain times, while the delay-and-sum beamformer sums whole signals with the delay. That is, the delay-and-sum beamformer includes both the pulse and other noises in its output, while the hyperbolic Radon transform can only sum the pulses

that result in a higher SNR for the pulsive signal.

When the travel time $\tau(\xi_1, \boldsymbol{\theta})$ is close to the true travel time, the hyperbolic Radon transform yields a large value by summing all pulses corresponding to the direct sound. In other words, $(Rd)(\boldsymbol{\theta})$ contains a peak at $\boldsymbol{\theta}$ corresponding to a proper parameter. Therefore, the estimation problem of a suitable parameter $\hat{\boldsymbol{\theta}}$ is formulated as the following maximization problem: find

$$\hat{\boldsymbol{\theta}} \in \arg\max_{\boldsymbol{\theta}} (Rd)(\boldsymbol{\theta}). \tag{4}$$

This type of maximization problem often arises in position estimation such as by beamforming. The standard method for solving Eq. (4) is an exhaustive search, where $(Rd)(\boldsymbol{\theta})$ is calculated for every candidate value of the parameters. However, as the sound speed is contained in the parameters, it is unsuitable for this problem because of the prohibitively large number of candidate solutions. Therefore, in the proposed method, a gradient-based optimization method is chosen to efficiently solve Eq. (4). Nevertheless, because the obtained signals are discretized signals, as shown in Fig. 2, the gradient of $(Rd)(\boldsymbol{\theta})$ cannot be derived symbolically from Eq. (3). Thus, a functional approximation is utilized in order to interpolate the discrete signals as a continuous function.

3.2. Continuous Interpolation by Functional Approximation

In the previous subsection, the parameter estimation problem was formulated as the maximization problem of $(Rd)(\boldsymbol{\theta})$. While $(Rd)(\boldsymbol{\theta})$ is calculated from the continuous signals $d_m(t)$ in Eq. (3), the obtained signals are discretized signals. Therefore, reconstruction of the continuous signal from the discrete signal by the interpolation is needed in order to calculate Eq. (3). Additionally, the derivation of the gradient of $(Rd)(\boldsymbol{\theta})$ should be taken into consideration in the interpolation. In the proposed method, signal interpolation using the spherical Bessel function of the first kind is employed since its derivative can be written simply.

A continuous signal $d_m(t)$ reconstructed from a discrete signal bandlimited to the Nyquist frequency is formulated as [38]

$$d_m(t) \simeq \sum_{n=1}^{N} d_m\left(\frac{n-1}{f_\mathrm{s}}\right) \mathrm{sinc}(f_\mathrm{s} t - n + 1), \tag{5}$$

where f_s is the sampling frequency and $\mathrm{sinc}(t)$ is the sinc function defined as

$$\mathrm{sinc}(t) = \begin{cases} \dfrac{\sin(\pi t)}{\pi t} & (t \neq 0) \\ 1 & (t = 0) \end{cases}. \tag{6}$$

Here, the spherical Bessel function of the first kind is introduced, which is denoted as $j_\nu(t)$ and given by

$$j_\nu(t) = \sqrt{\frac{\pi}{2t}} J_{\nu+1/2}(t), \tag{7}$$

where $J_\nu(t)$ is the Bessel function of the first kind defined by

$$J_\nu(t) = \left(\frac{t}{2}\right)^\nu \sum_{k=0}^{\infty} \frac{1}{k!\,\Gamma(\nu + k + 1)} \left(\frac{-t^2}{4}\right)^k \tag{8}$$

and $\Gamma(t)$ is the gamma function

$$\Gamma(t) = \int_0^\infty z^{t-1} e^{-z} dz. \tag{9}$$

Using the following property of the spherical Bessel function of the first kind,

$$j_0(\pi t) = \mathrm{sinc}(t), \tag{10}$$

Eq. (5) becomes

$$d_m(t) \simeq \sum_{n=1}^{N} d_m\left(\frac{n-1}{f_\mathrm{s}}\right) j_0(\pi(f_\mathrm{s} t - n + 1)), \tag{11}$$

which can be rewritten in a matrix form as

$$d_m(t) \simeq \boldsymbol{d}_m^\mathrm{T} \boldsymbol{j}_0(t), \tag{12}$$

where

$$\boldsymbol{d}_m = \left[d_m(0) \ldots d_m\left(\frac{N-1}{f_\mathrm{s}}\right) \right]^\mathrm{T},$$
$$\boldsymbol{j}_\nu(t) = [j_\nu(\pi f_\mathrm{s} t) \ldots j_\nu(\pi(f_\mathrm{s} t - N + 1))]^\mathrm{T}.$$

From Eq. (12), the continuous signal $d_m(t)$ is reconstructed from the discrete signal $\boldsymbol{d}_m$. When Eq. (12) is substituted into Eq. (3), $(Rd)(\boldsymbol{\theta})$ becomes

$$(Rd)(\boldsymbol{\theta}) = \boldsymbol{d}^\mathrm{T} \boldsymbol{J}_0(\boldsymbol{\theta}), \tag{13}$$

where

$$\boldsymbol{d} = [\boldsymbol{d}_1^\mathrm{T} \ldots \boldsymbol{d}_M^\mathrm{T}]^\mathrm{T},$$
$$\boldsymbol{J}_\nu(\boldsymbol{\theta}) = [\boldsymbol{j}_\nu(\tau(h_1, \boldsymbol{\theta}))^\mathrm{T} \ldots \boldsymbol{j}_\nu(\tau(h_M, \boldsymbol{\theta}))^\mathrm{T}]^\mathrm{T}.$$

Therefore, $(Rd)(\boldsymbol{\theta})$ can be calculated from the discrete data $\boldsymbol{d}$ using Eq. (13).

3.3. Maximization by Gradient-based Optimization Method

In order to solve Eq. (4) by the gradient-based optimization method, the gradient of $(Rd)(\boldsymbol{\theta})$ is derived in this subsection. Then, a description of Nesterov's accelerated gradient method used to solve Eq. (4) is given.

From Eq. (13), the gradient of $(Rd)(\boldsymbol{\theta})$, denoted as $\mathrm{grad}(Rd)(\boldsymbol{\theta})$, is formulated as

$$\begin{aligned} \mathrm{grad}(Rd)(\boldsymbol{\theta}) &= \mathcal{J}((Rd)(\boldsymbol{\theta}), \boldsymbol{\theta})^\mathrm{T} \\ &= \mathcal{J}(\boldsymbol{J}_0(\boldsymbol{\theta}), \boldsymbol{\theta})^\mathrm{T} \boldsymbol{d}, \end{aligned} \tag{14}$$

where $\mathcal{J}(\boldsymbol{f}, \boldsymbol{\phi})$ is the Jacobian matrix defined by

$$\mathcal{J}(\boldsymbol{f},\boldsymbol{\phi}) = \begin{bmatrix} \frac{\partial f_1}{\partial \phi_1} & \cdots & \frac{\partial f_1}{\partial \phi_N} \\ \vdots & \ddots & \vdots \\ \frac{\partial f_M}{\partial \phi_1} & \cdots & \frac{\partial f_M}{\partial \phi_N} \end{bmatrix}. \tag{15}$$

The spherical Bessel function of the first kind of order zero can be derived as follows:

$$\frac{\partial j_0(t)}{\partial t} = -j_1(t). \tag{16}$$

Therefore,

$$\mathcal{J}(\boldsymbol{J}_0(\boldsymbol{\theta}),\boldsymbol{\theta}) = -\pi f_s \,\mathrm{diag}(\boldsymbol{J}_1(\boldsymbol{\theta}))\mathcal{J}(\boldsymbol{\tau}_{\mathrm{rep}}(\boldsymbol{\theta}),\boldsymbol{\theta}), \tag{17}$$

where

$$\boldsymbol{\tau}_{\mathrm{rep}}(\boldsymbol{\theta}) = \boldsymbol{\tau}(\boldsymbol{\theta}) \otimes \mathbf{1}_N,$$
$$\boldsymbol{\tau}(\boldsymbol{\theta}) = [\tau(h_1,\boldsymbol{\theta}) \ldots \tau(h_M,\boldsymbol{\theta})]^{\mathrm{T}},$$

$\mathrm{diag}(\boldsymbol{x})$ is a square diagonal matrix with the elements of $\boldsymbol{x}$ on the main diagonal, $\otimes$ is the Kronecker product operator, and $\mathbf{1}_N$ is the all-ones column vector of dimension N. That is, $\boldsymbol{x} \otimes \mathbf{1}_N$ is a column vector repeating each element of $\boldsymbol{x}$ (N times) when $\boldsymbol{x}$ is a column vector. Then, $\mathcal{J}(\boldsymbol{\tau}_{\mathrm{rep}}(\boldsymbol{\theta}),\boldsymbol{\theta})$ is given by

$$\mathcal{J}(\boldsymbol{\tau}_{\mathrm{rep}}(\boldsymbol{\theta}),\boldsymbol{\theta}) = \mathcal{J}(\boldsymbol{\tau}(\boldsymbol{\theta}),\boldsymbol{\theta}) \otimes \mathbf{1}_N,$$

and each element of $\mathcal{J}(\boldsymbol{\tau}(\boldsymbol{\theta}),\boldsymbol{\theta})$ is

$$\frac{\partial}{\partial s_{\xi_1}}\tau(h_m,\boldsymbol{\theta}) = p\frac{s_{\xi_1} - h_m}{\sqrt{(s_{\xi_1} - h_m)^2 + s_{\xi_2}^2}},$$
$$\frac{\partial}{\partial s_{\xi_2}}\tau(h_m,\boldsymbol{\theta}) = p\frac{s_{\xi_2}}{\sqrt{(s_{\xi_1} - h_m)^2 + s_{\xi_2}^2}},$$
$$\frac{\partial}{\partial p}\tau(h_m,\boldsymbol{\theta}) = \sqrt{(s_{\xi_1} - h_m)^2 + s_{\xi_2}^2}. \tag{18}$$

Thus, $\mathrm{grad}(Rd)(\boldsymbol{\theta})$ is calculated by Eqs. (14), (17), and (18).

As the gradient-based optimization method used to solve Eq. (4), Nesterov's accelerated gradient method, which is a first-order optimization method with a better convergence rate than the gradient descent method, is chosen [39,40]. In Nesterov's method, Eq. (4) is solved by the following iterative procedure:

$$\boldsymbol{v}_{k+1} = \mu\boldsymbol{v}_k + \alpha\,\mathrm{grad}(Rd)(\boldsymbol{\theta}_k + \mu\boldsymbol{v}_k)$$
$$\boldsymbol{\theta}_{k+1} = \boldsymbol{\theta}_k + \boldsymbol{v}_{k+1}, \tag{19}$$

where k is the iteration index, $\alpha > 0$ is the step size, $\mu \in [0,1]$ is the momentum coefficient, and $\boldsymbol{v}_i$ is the velocity vector. These additional momentum and velocity terms accelerate the update of parameters, which can improve the accuracy of the estimation, especially when the objective function is nearly flat around the optimal value as in this case. Note that in this algorithm, one does not have to calculate $(Rd)(\boldsymbol{\theta})$ to solve Eq. (4) because $\mathrm{grad}(Rd)(\boldsymbol{\theta})$ is directly calculated through the functional approximation.

Table 1 Simulation conditions for seismic migration.

Number of receivers M	100
Interval of receivers [m]	12.5
Interval of shots [m]	12.5
Number of shots	81
Recording time [s]	6.5
Sampling rate f_s [Hz]	1,000
RMSE of positions [m]	$10^{-3}, 10^{-2.5}, \ldots, 10^{1}$
Type of emitted signal	linear chirp signal
Frequency range of signal [Hz]	10–100

4. NUMERICAL SIMULATION

Two numerical simulation experiments were performed in order to show the effectiveness of the proposed method. First, an experiment to investigate the influence of the error of the sound source position on seismic imaging was performed. This experiment provides the required accuracy of source localization in a seismic survey. Then, to confirm the localization accuracy of the proposed method, it was applied to simulated data and compared with the Cramér–Rao lower bound.

4.1. Influence of Localization Accuracy on Seismic Imaging

In this subsection, an experiment involving seismic migration was performed to confirm the influence of the localization accuracy. Because the subsurface reflector positions are measured from the appearances of migrated images, the results of the localization should also be evaluated from the appearances. The experiment provides an acceptable error for seismic migration evaluated from migrated images.

Seismic migration using source positions, which deviated from the correct positions with different root mean square errors (RMSEs), was applied to the simulated data. Then, the SNR of these migrated images was calculated. The simulation conditions are shown in Table 1. The finite-difference time-domain (FDTD) method was used for the calculation, and an upward linear chirp signal with a duration of 4 s was emitted from the source position. For the velocity model, part of the Marmousi2 velocity model [41] was used, and the velocity distribution for the migration was the same as the velocity model of the simulation.

To obtain the migrated images, Kirchhoff prestack depth migration [42,43] was used in the experiment. This is one of the popular migration methods, which relocates the energy of reflected waves in the depth domain, on the basis of the Kirchhoff integral solution of the acoustic wave equation. The migrated image $I(\xi_1,\xi_2)$ is calculated using

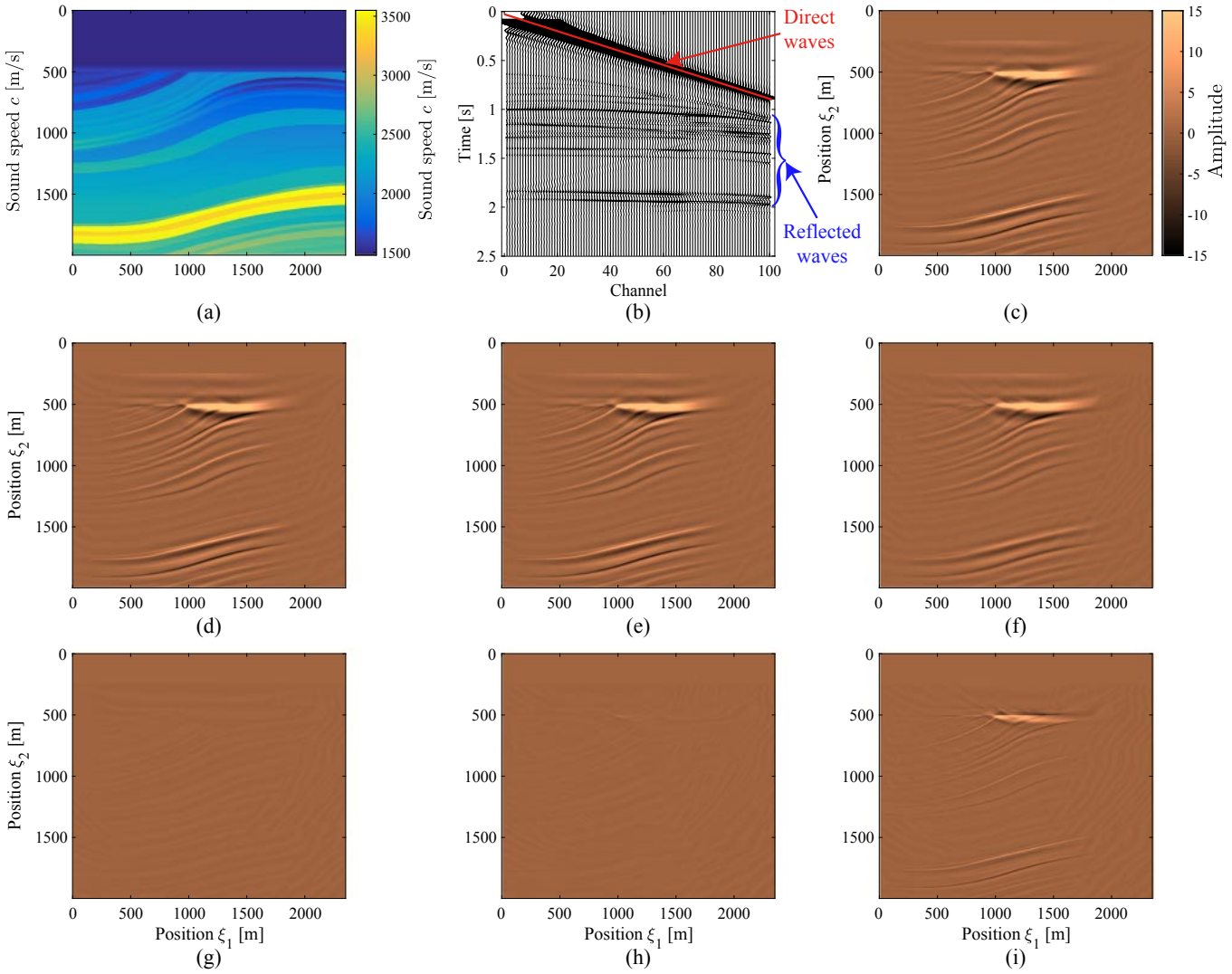

Fig. 3 Velocity model and migration results. (a) Part of the Marmousi2 velocity model [41], which is used in the simulation. (b) Simulated signals of the first shot pulse-compressed by the cross-correlation of the emitted signal and observed signals. (c) Migrated image, I_c, obtained with correct source positions from the simulated signals. (d), (e), and (f) Migrated images, I_σ, obtained with RMSEs of the positions of 10^{-1} m, 10^0 m, and 10^1 m, respectively. (g), (h), and (i) Residual images of (d), (e), and (f), calculated as $I_c - I_\sigma$, respectively.

$$I(\xi_1, \xi_2) = \sum_i \sum_m d_m^{(i)}(t_{\mathrm{s}}^{(i)}(\xi_1, \xi_2) + t_{\mathrm{r}}^{(i)}(m, \xi_1, \xi_2)), \quad (20)$$

where $d_m^{(i)}$ is the data obtained by the mth receiver for the ith shot, t_{s} is the travel time from the source to the point (ξ_1, ξ_2), and t_{r} is the travel time from the point (ξ_1, ξ_2) to the receivers.

Figure 3 shows the velocity model and migration results. Note that both the left and right edges of the migrated images are not clear owing to the shortage of reflected waves. Figure 3(c) was migrated with the correct source positions, while Figs. 3(d)–3(f) were migrated with erroneous source positions whose RMSEs were 10^{-1} m, 10^0 m, and 10^1 m, respectively. Here, the errors of the positions were measured as the RMSE because 81 shots (thus, 81 source positions) were necessary to construct a single migrated image for this setting (Table 1). In the figures, there is little noticeable difference between Figs. 3(c), 3(d), and 3(e). However, Fig. 3(f) and its error in Fig. 3(i) indicate that there is an influence on the seismic migration when the RMSE of the positions is 10^1 m.

The SNR of migrated images was calculated as

$$\mathrm{SNR}_{\mathrm{mig}} = 10 \log_{10} \frac{\|I_c\|_{\mathrm{F}}^2}{\|I_c - I_\sigma\|_{\mathrm{F}}^2}, \quad (21)$$

where I_c is the migrated image obtained from the correct source positions using the simulated data, I_σ is the migrated image obtained from erroneous source positions with RMSE σ, and $\|\cdot\|_{\mathrm{F}}$ is the Frobenius norm. $\mathrm{SNR}_{\mathrm{mig}}$ for each RMSE is shown in Fig. 4. When the RMSE of the positions is 10^0 m, $\mathrm{SNR}_{\mathrm{mig}}$ is approximately 60 dB. In addition, $\mathrm{SNR}_{\mathrm{mig}}$ monotonically decreases as the RMSE of

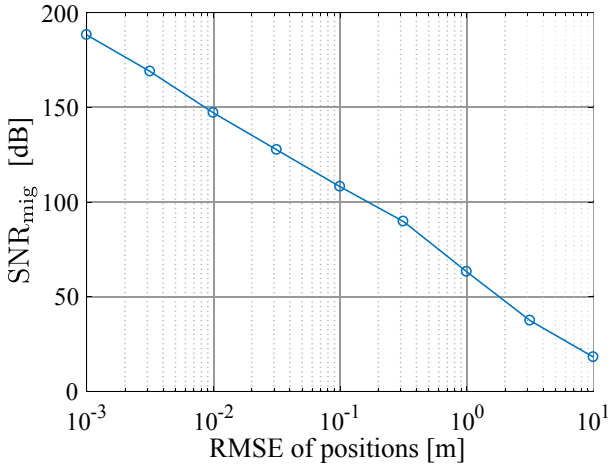

Fig. 4 SNR of migrated images versus RMSE of source positions.

the positions increases. These results indicate that there is no visual influence on the seismic migration when the RMSE of the deviated source position is less than 10^0 m.

4.2. Estimation Accuracy of Proposed Method

In the previous subsection, the influence of the localization accuracy on seismic migration images was investigated. In this subsection, the localization accuracy of the proposed method is shown in order to confirm that the localization accuracy is sufficient for seismic migration. The proposed method was applied to simulated data with different SNRs, and the RMSE of the estimated parameter $\hat{\boldsymbol{\theta}}$ was calculated. Then, the RMSE was compared with the Cramér–Rao lower bound (CRLB), which is a theoretical lower bound for the variance of any unbiased estimator [44,45].

The simulation conditions of the source localization experiment are shown in Table 2. The emitted signal was the same as in the previous experiment (linear chirp of 10–100 Hz). The SNR of obtained signals was calculated as

$$\mathrm{SNR}_{\mathrm{signal}} = 10\log_{10}\frac{\sum_{m=1}^{M}\|\boldsymbol{x}_m\|_2^2}{\sum_{m=1}^{M}\|\boldsymbol{w}_m\|_2^2}, \tag{22}$$

where $\boldsymbol{x}_m$ is the data obtained from the mth receiver without noise, $\boldsymbol{w}_m$ is additive Gaussian noise with variance σ^2, and $\|\cdot\|_2$ is the ℓ_2 norm.

One example of a slice of $(Rd)(\boldsymbol{\theta})$ calculated by Eq. (13) and distributions of the estimated parameter of each plane when $\mathrm{SNR}_{\mathrm{signal}}$ is 0 dB are shown in Fig. 5. (★) and (○) represent the correct estimation parameter and the estimated parameters $\hat{\boldsymbol{\theta}}$, respectively. The mean of $|(Rd)(\boldsymbol{\theta})|$ integrated along the depth direction for each plane is shown in Fig. 6, where the absolute value was taken to avoid cancellation. Note that Fig. 6 illustrates the mean of the depth information because Fig. 5 is merely a slice of $(Rd)(\boldsymbol{\theta})$ that does not give information in the depth direction.

Table 2 Simulation conditions for source localization.

Number of receivers M	100
Interval of receivers [m]	12.5
Correct estimation parameter	$[90\ 60\ 1{,}510]^{\mathrm{T}}$
Initial parameter for estimation	$[100\ 50\ 1{,}500]^{\mathrm{T}}$
Recording time [s]	7.0
Sampling rate f_s [Hz]	1,000
$\mathrm{SNR}_{\mathrm{signal}}$ [dB]	$-20, -15, \ldots, 50$
Number of trials	1,000 for each $\mathrm{SNR}_{\mathrm{signal}}$

From Fig. 5, it can be seen that the value of $(Rd)(\boldsymbol{\theta})$ had a peak around the correct parameter, and the estimated parameters were concentrated around the correct parameter. The direction of the spread of the estimated parameters was consistent with the direction of the peaks for the s_{ξ_1}-s_{ξ_2} and s_{ξ_1}-c slices, but not for the c-s_{ξ_2} slice. The reason for this result can be seen from Fig. 6, where the direction of the spread in the mean value of the c-s_{ξ_2} plane is different from that of the single slice in Fig. 5. That is, the spread of the peak of $(Rd)(\boldsymbol{\theta})$ in the c-s_{ξ_2} plane may occur in several directions, which resulted in the direction of the spread of the estimated parameters.

Note that although $(Rd)(\boldsymbol{\theta})$ has several local maxima, it can be determined from the value of $(Rd)(\hat{\boldsymbol{\theta}})$ whether the obtained parameter $\hat{\boldsymbol{\theta}}$ is the globally optimal maximum. Since the hyperbolic Radon transform is simply the summation of data values, the global maximum of $(Rd)(\boldsymbol{\theta})$ must be close to the summation of each maximal value of the observed signal. Therefore, because the global maximum and local maxima have considerably different values, as shown in Fig. 5, one can decide whether the obtained parameter is globally optimum by comparing $(Rd)(\hat{\boldsymbol{\theta}})$ and the sum of the maximum values of the observed signals. If the obtained parameter is suspected of being a trapped solution of a local maximum, then one can try another initial value until a likely global solution is obtained.

For comparison, the results of estimation by the MUSIC method are shown in Fig. 7. The sound speed was set to the correct value, and only the position was estimated from the MUSIC spectrum, which was maximized by an exhaustive search. The MUSIC method obtained a reasonably good estimate for the direction as there was only one sound source. On the other hand, although the sound speed had no error and all the frequencies of the signal (10–100 Hz) were utilized, it had a rather wide dispersion of the distance, which is known as a general phenomenon [46,47]. This comparison indicates that this simulation is a difficult situation for

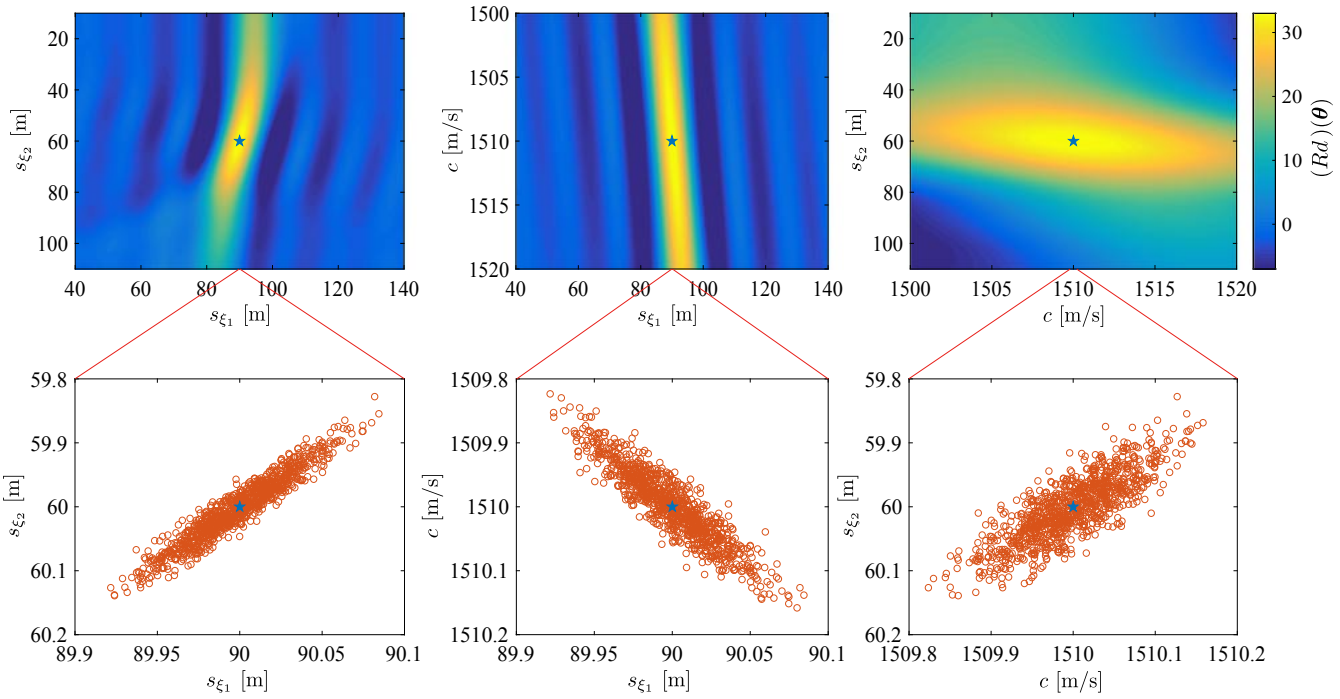

Fig. 5 Example of values of $(Rd)(\boldsymbol{\theta})$ (top), and distributions of the estimated parameters of all trials for each plane when $\mathrm{SNR}_{\mathrm{signal}}$ was 0 dB (bottom). (★) and (○) represent the correct estimation parameter and the estimated parameters $\hat{\boldsymbol{\theta}}$, respectively. The RMSEs for these results and for the other SNR values are summarized in Fig. 8.

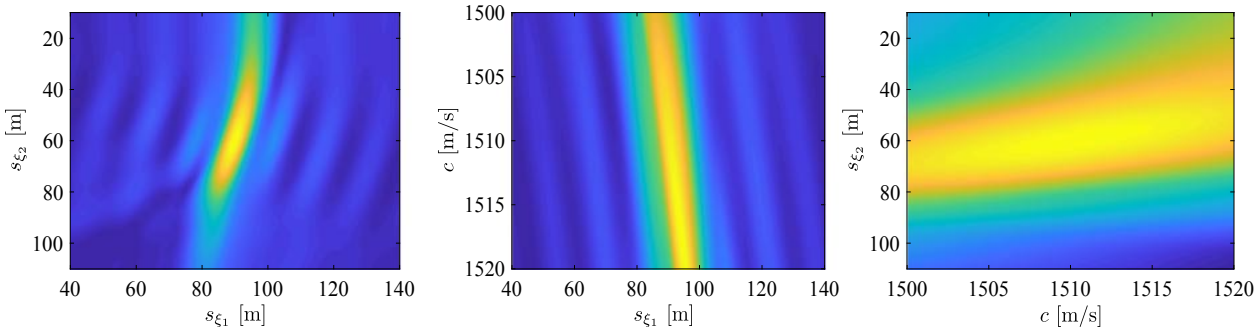

Fig. 6 Mean of $|(Rd)(\boldsymbol{\theta})|$ integrated along the depth direction in Fig. 5.

accurately localizing the source position even when the exact sound speed is known.

Then, the proposed method was compared with the theoretical lower bound. The RMSEs of the estimated parameters $\hat{\boldsymbol{\theta}}$ for each $\mathrm{SNR}_{\mathrm{signal}}$ are summarized in Fig. 8, where the CRLB is also depicted. Each color represents a different element of the parameter vector. The solid lines correspond to the RMSE of the estimated parameters, and the dashed lines indicate the CRLB. As shown in the figure, the RMSE of each estimated parameter almost reached the CRLB of each parameter, which indicates that the proposed method is unbiased. Moreover, even when $\mathrm{SNR}_{\mathrm{signal}}$ was -20 dB, the RMSE of the estimated parameter $\hat{\boldsymbol{\theta}}$ was less than 10^0 m. Thus, the proposed method provides sufficient accuracy for the seismic migration according to Fig. 4 since the positional error of 10^0 can hardly be observed visually as shown in Fig. 3.

The estimated results for different sampling intervals were also investigated, as shown in Fig. 9, to test the proposed method under different conditions. The intervals of the receivers were halved (6.25 m) and doubled (25 m). These figures illustrate that the proposed method also almost reached the CRLB for these sensor intervals. For all cases in these experiments, the errors of the position were less than 10^0 m, which is sufficiently accurate in terms of migrated images for these situations. We should note, however, that these results were obtained for an ideal situation, i.e., additive Gaussian noise. Real data will contain some non-Gaussian noise, and therefore these results should be interpreted with that in mind.

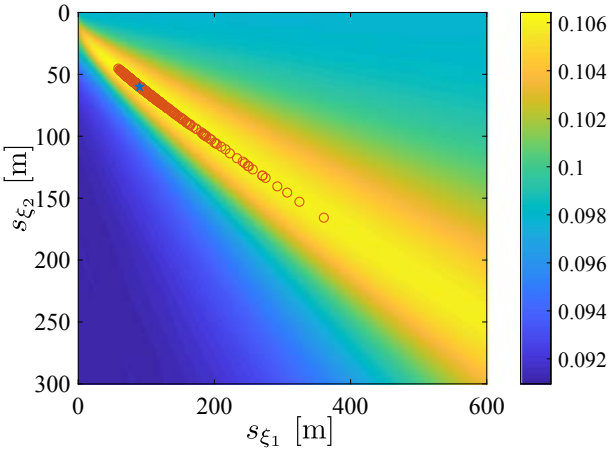

Fig. 7 Example of the MUSIC spectrum and distributions of the parameters estimated by the MUSIC method. $\mathrm{SNR}_{\mathrm{signal}}$ was 0 dB and the results of 1,000 trials are plotted.

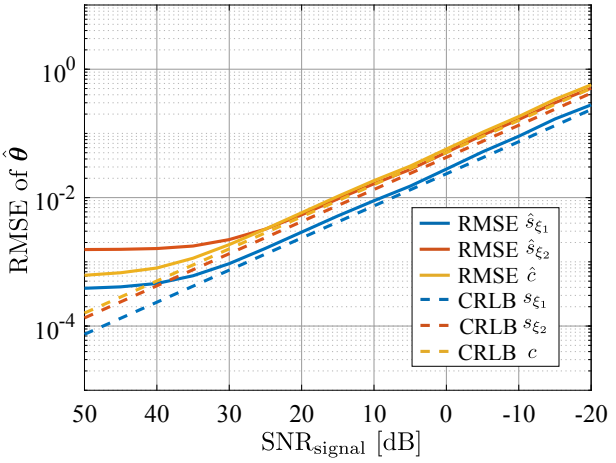

Fig. 8 RMSE of estimated parameter $\hat{\boldsymbol{\theta}}$ versus SNR of obtained signals. Each color represents a different element of the parameter vector. The solid lines indicate the RMSE of the estimated parameters, and the dashed lines indicate the CRLB.

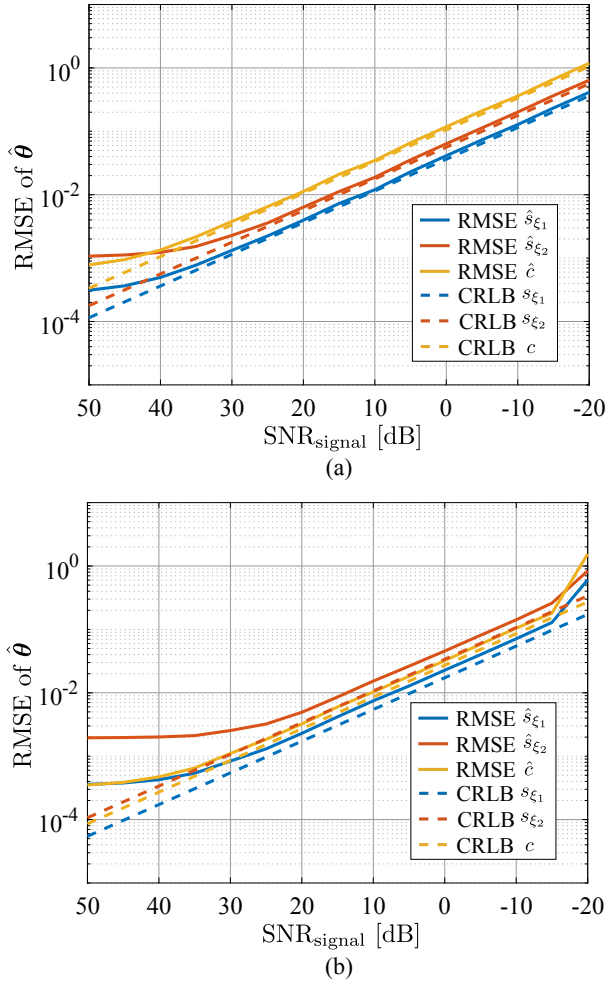

Fig. 9 RMSE of the estimated parameter $\hat{\boldsymbol{\theta}}$ and the CRLB for each $\mathrm{SNR}_{\mathrm{signal}}$ when the intervals of the receivers were (a) 6.25 m, and (b) 25 m.

5. CONCLUSION

In this paper, a sound source localization method using seismic data via hyperbolic Radon transform was proposed. The parameter estimation problem was formulated as a maximization problem using the hyperbolic Radon transform, which integrates the seismic data along the travel time, and it was solved by Nesterov's accelerated gradient method with continuous interpolation using the spherical Bessel function of the first kind. The numerical simulations showed the localization accuracy required for seismic migration, which is achieved by the proposed method. The comparison of these results confirmed that the proposed method is able to achieve the accuracy required in seismic migration even when the SNR of the observed signal is −20 dB for additive Gaussian noise.

Although the performance of the proposed method was confirmed by several simulations, it was only examined for the case of additive Gaussian noise. In the real measurement in a marine seismic survey, there will be some non-Gaussian noise, which will reduce the accuracy of the parameter estimation. Therefore, an evaluation of the proposed method under real conditions should be performed as a future work. In addition, the sound speed was assumed to be constant on the basis of the operable depth of an MSV. The proposed method should be improved so that it can be utilized at deeper positions where the shallow-water assumption no longer holds. Therefore, an extension of the proposed method to a nonconstant sound speed should be considered with the development of MSVs.

REFERENCES

[1] M. T. Taner and F. Koehler, "Velocity spectra — digital computer derivation applications of velocity functions," *Geophysics*, **34**, 859–881 (1969).

[2] P. Carrion, "Reflection tomography in underwater acoustics," *J. Acoust. Soc. Am.*, **97**, 1318–1321 (1995).

[3] B. Marsset, T. Missiaen, Y.-H. De Roeck, M. Noble, W. Versteeg and J. Henriet, "Very high resolution 3D marine seismic data processing for geotechnical applications," *Geophys. Prospect.*, **46**, 105–120 (1998).
[4] B. Duquet, K. J. Marfurt and J. A. Dellinger, "Kirchhoff modeling, inversion for reflectivity, and subsurface illumination," *Geophysics*, **65**, 1195–1209 (2000).
[5] Y. Sun, F. Qin, S. Checkles and J. P. Leveille, "3-D prestack Kirchhoff beam migration for depth imaging," *Geophysics*, **65**, 1592–1603 (2000).
[6] O. C. Rodríguez and S. M. Jesus, "Physical limitations of travel-time-based shallow water tomography," *J. Acoust. Soc. Am.*, **108**, 2816–2822 (2000).
[7] R. M. Shipp and S. C. Singh, "Two-dimensional full wavefield inversion of wide-aperture marine seismic streamer data," *Geophys. J. Int.*, **151**, 325 (2002).
[8] W. Dai, Y. Huang and G. T. Schuster, "Least-squares reverse time migration of marine data with frequency-selection encoding," *Geophysics*, **78**, S233–S242 (2013).
[9] J. E. Barger and W. R. Hamblen, "The air gun impulsive underwater transducer," *J. Acoust. Soc. Am.*, **68**, 1038–1045 (1980).
[10] B. Dragoset, "Introduction to air guns and air-gun arrays," *Leading Edge*, **19**, 892–897 (2000).
[11] J. Gordon, D. Gillespie, J. Potter, A. Frantzis, M. P. Simmonds, R. Swift and D. Thompson, "A review of the effects of seismic surveys on marine mammals," *Mar. Technol. Soc. J.*, **37**, 16–34 (2003).
[12] R. D. McCauley, J. Fewtrell and A. N. Popper, "High intensity anthropogenic sound damages fish ears," *J. Acoust. Soc. Am.*, **113**, 638–642 (2003).
[13] R. A. Broding, J. M. Hess and R. E. Wanous, "A high-power computer-controlled marine Vibroseis system," *IEEE Trans. Geosci. Electron.*, **9**, 90–95 (1971).
[14] H. C. Hardee and R. G. Hills, "The resonant acoustic pulser — A continuous-frequency marine seismic source," *Geophysics*, **48**, 1082–1089 (1983).
[15] H. Ozasa, H. Mikada, F. Sato, F. Murakami, J. Takekawa and E. Asakawa, "Development of hydraulic low frequency marine seismic vibrator," *Proc. 19th Int. Symp. Recent Adv. Explor. Geophys.* (*RAEG*), ID: STT13–14 (2015).
[16] H. Ozasa, F. Sato, E. Asakawa, F. Murakami, E. J. Hondori, J. Takekawa and H. Mikada, "Development of marine seismic vibrator towards realization of shear wave source with no touch-down to seafloor," *Int. Pet. Tech. Conf.*, ID: IPTC–18903–MS (2016).
[17] K. Vickery, "Acoustic positioning systems. A practical overview of current systems," *Proc. IEEE 1998 Workshop Auton. Underw. Veh.*, pp. 5–17 (1998).
[18] H.-P. Tan, R. Diamant, W. K. Seah and M. Waldmeyer, "A survey of techniques and challenges in underwater localization," *Ocean Eng.*, **38**, 1663–1676 (2011).
[19] L. Paull, S. Saeedi, M. Seto and H. Li, "AUV navigation and localization: A review," *IEEE J. Oceanic Eng.*, **39**, 131–149 (2014).
[20] R. Kaune, "Accuracy studies for TDOA and TOA localization," *15th Int. Conf. Information Fusion*, pp. 408–415 (2012).
[21] H. Krim and M. Viberg, "Two decades of array signal processing research: The parametric approach," *IEEE Signal Process. Mag.*, **13**, 67–94 (1996).
[22] J. M. Ozard, "Matched field processing in shallow water for range, depth, and bearing determination: Results of experiment and simulation," *J. Acoust. Soc. Am.*, **86**, 744–753 (1989).
[23] A. B. Baggeroer, W. A. Kuperman and P. N. Mikhalevsky, "An overview of matched field methods in ocean acoustics," *IEEE J. Oceanic Eng.*, **18**, 401–424 (1993).
[24] T. Kusano, K. Yatabe, Y. Oikawa, H. Ozasa, K. Tanaka and F. Sato, "Estimation of position of marine seismic vibrator via hyperbolic Radon transform," *Proc. Autumn Meet. Acoust. Soc. Jpn.*, pp. 1085–1086 (2016) (in Japanese).
[25] Ö. Yilmaz, *Seismic Data Analysis* (Society of Exploration Geophysicists, Tulsa, 2001).
[26] M. R. Gadallah and R. Fisher, *Exploration Geophysics* (Springer-Verlag, Berlin/Heidelberg, 2008).
[27] F.-X. Han, J.-G. Sun and K. Wang, "The influence of sea water velocity variation on seismic traveltimes, ray paths, and amplitude," *Appl. Geophys.*, **9**, 319–325 (2012).
[28] S. D. Blunt and K. Gerlach, "Adaptive pulse compression via MMSE estimation," *IEEE Trans. Aerosp. Electron. Syst.*, **42**, 572–584 (2006).
[29] T. Kusano, K. Yatabe, Y. Oikawa, H. Ozasa, K. Tanaka and F. Sato, "Pulse compression method using sparse optimization for seafloor resources exploration," *Proc. Spring Meet. Acoust. Soc. Jpn.*, pp. 1321–1322 (2017) (in Japanese).
[30] S. Deans, *The Radon Transform and Some of Its Applications* (Wiley, New York, 1983).
[31] C. H. Chapman, "Generalized Radon transforms and slant stacks," *Geophys. J. Int.*, **66**, 445 (1981).
[32] W. S. Harlan, J. F. Claerbout and F. Rocca, "Signal/noise separation and velocity estimation," *Geophysics*, **49**, 1869–1880 (1984).
[33] J. R. Thorson and J. F. Claerbout, "Velocity-stack and slant-stack stochastic inversion," *Geophysics*, **50**, 2727–2741 (1985).
[34] I. Tsvankin and L. Thomsen, "Nonhyperbolic reflection moveout in anisotropic media," *Geophysics*, **59**, 1290–1304 (1994).
[35] D. Trad, T. Ulrych and M. Sacchi, "Latest views of the sparse Radon transform," *Geophysics*, **68**, 386–399 (2003).
[36] J. Wang, M. Ng and M. Perz, "Seismic data interpolation by greedy local Radon transform," *Geophysics*, **75**, WB225–WB234 (2010).
[37] J. Hu, S. Fomel, L. Demanet and L. Ying, "A fast butterfly algorithm for generalized Radon transforms," *Geophysics*, **78**, U41–U51 (2013).
[38] M. Unser, "Sampling-50 years after Shannon," *Proc. IEEE*, **88**, 569–587 (2000).
[39] Y. Nesterov, "A method of solving a convex programming problem with convergence rate $\mathcal{O}(1/k^2)$," *Sov. Math. Dokl.*, **27**, 372–376 (1983).
[40] I. Sutskever, J. Martens, G. Dahl and G. Hinton, "On the importance of initialization and momentum in deep learning," *Proc. 30th Int. Conf. Mach. Learn.* (*ICML*), Vol. 28, pp. 1139–1147 (2013).
[41] G. S. Martin, R. Wiley and K. J. Marfurt, "Marmousi2: An elastic upgrade for Marmousi," *Leading Edge*, **25**, 156–166 (2006).
[42] S. H. Gray and W. P. May, "Kirchhoff migration using eikonal equation traveltimes," *Geophysics*, **59**, 810–817 (1994).
[43] J. Zhu and L. R. Lines, "Comparison of Kirchhoff and reverse-time migration methods with applications to prestack depth imaging of complex structures," *Geophysics*, **63**, 1166–1176 (1998).
[44] S. M. Kay, *Fundamentals of Statistical Signal Processing: Estimation Theory* (Prentice Hall, Upper Saddle River, N.J., 1993).
[45] J. C. Chen, R. E. Hudson and K. Yao, "Maximum-likelihood source localization and unknown sensor location estimation for wideband signals in the near-field," *IEEE Trans. Signal*

Process., **50**, 1843–1854 (2002).
[46] J. Liang and D. Liu, "Passive localization of mixed near-field and far-field sources using two-stage music algorithm," *IEEE Trans. Signal Process.*, **58**, 108–120 (2010).
[47] T. Tachikawa, K. Yatabe, Y. Ikeda and Y. Oikawa, "Sound source localization based on sparse estimation and convex clustering," *5th Jt. Meet. Acoust. Soc. Am. Acoust. Soc. Jpn.*, Vol. 140, pp. 3195–3196 (2016).

Tsubasa Kusano received his B.E. degree from Waseda University in 2017. He is currently pursuing an M.E. degree at the Department of Intermedia Art and Science, Waseda University. His research interests include signal processing based on functional approximation and functional data analysis.

Kohei Yatabe received his B.E., M.E., and Ph.D. degrees from Waseda University in 2012, 2014, and 2017, respectively. He is currently an assistant professor of the Department of Intermedia Art and Science, Waseda University. His research interests include optical and acoustical signal processing.

Yasuhiro Oikawa received his B.E., M.E., and Ph.D. degrees in Electrical Engineering from Waseda University in 1995, 1997, and 2001, respectively. He is a professor of the Department of Intermedia Art and Science, Waseda University. His main research interests are communication acoustics and digital signal processing of acoustic signals. He is a member of ASJ, ASA, IEICE, IEEE, IPSJ, VRSJ, and AIJ.